Analysis of a Novel Transverse Flux Generator in Direct-driven Wind Turbines

Dmitry Svechkarenko, Juliette Soulard, and Chandur Sadarangani

***Abstract*— This paper presents analysis of a novel transverse flux direct-driven wind generator. The analytical model for the calculation of different parts of the inductance is developed and applied for the evaluation of machine performance with respect to its geometry. Generators rated for 3, 5, 7, and 10 MW output power are investigated. The possible ranges of design parameters are discussed and conclusions are drawn.**

***Index Terms*— Direct-driven wind turbine, inductance model, permanent magnet, transverse flux machine.**

I. Introduction

With the further development of wind energy and increased wind power penetration level in power systems, the issues of availability and reliability of generating units become of great importance. This particularly applies for stand-alone and offshore applications due to their often hard-to-reach locations. The overall reliability of wind turbine is somewhat reduced by using a gearbox, which is applied for adjustment of a low-speed turbine shaft to a higher rotational speed of a conventional generator. In addition, a gearbox is subject to mechanical wear, vibrations, requires lubrication and more frequent maintenance at considerable cost. As a result, a gearless wind energy system has drawn attention of wind turbine manufacturers (Enercon, Made, Harakosan). An overview of gearless system, as well as the components it comprises, is presented in Fig. 1.

As can be noticed, for the connection of a generator to the network, a converter scaled for the full output power is required. This would increase a system cost and introduce additional losses. On the other hand, a full-scaled converter has an opportunity of a variable speed control with a large range. This allows a better utilization of the available mechanical power and therefore has a potentially higher energy yield.

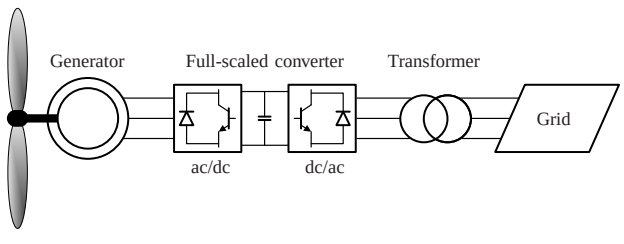

Fig. 1. A gearless wind energy system.

Manuscript received July 6, 2006.

D. Svechkarenko, J. Soulard, and C. Sadarangani are with the Electrical Machines and Power Electronics Laboratory, School of Electrical Engineering, Royal Institute of Technology, Teknikringen 33, 10044 Stockholm, Sweden (tel: +46 87907724, fax: +46 8205268, email: dmitrys@ee.kth.se).

An interest in gearless energy systems is likely to continue growing in the near future, as larger power converters become available.

A direct-driven low-speed generator with a large number of poles and larger than conventional generator output diameter is used in the gearless energy system. Electrically excited direct-driven synchronous and induction generators are utilized by a number of wind turbines manufacturers (Enercon, Made) [1]. In the last few years, a reduced magnet price made a synchronous generator with a permanent magnet excitation (PMSG) an attractive alternative. This topology, for example, is utilized by Harakosan in their 2 MW wind turbine. In comparison to the electrical excitation, the permanent magnet excitation favors a reduced active weight, decreased copper losses, yet the energy yield is somewhat higher [2].

A number of studies have been conducted to investigate different topologies of PMSG suited for direct-driven low-speed wind generators. A possibility of utilizing a transverse flux permanent magnet (TFPM) topology in the gearless wind energy system was discussed by Weh in [3]. An attractive feature of the TFPM is that with increasing number of poles, unlike in the radial flux machine, the current loading can be increased and as a result a higher value of specific torque density can be achieved [4].

This paper concentrates on the analysis of a novel TFPM topology and investigates its possible utilization in wind generators from 3 to 10 MW.

A. General Overview of a Novel TFPM Generator

The novel machine can be referred to as a rotational multiphase single-sided transverse flux machine without return paths [4], [5]. The cross-section of the TFPM generator geometry is presented in Fig. 2. As can be observed, the generator consists of a hollow toroidal rotor with surface-mounted permanent magnets embraced by the laminated stacks with the windings placed in the slots. The main machine radius R_m and the tube radius R_s are shown in Fig. 2. The cut required for the mechanical assembling of the rotor on the shaft is presented by angle $2\,\xi$.

The TFPM topology allows to use a stator winding of a simple mechanical structure, which facilitates high voltage insulation. This could be an attractive feature in the future since the voltage of wind generators has been continuously increasing in the voltage levels up to $5\,\mathrm{kV}$ can reasonably be expected in the forthcoming generators [6].

The arrangement presented in Fig. 3 was selected for the further analysis, as it has a shorter end-winding and is

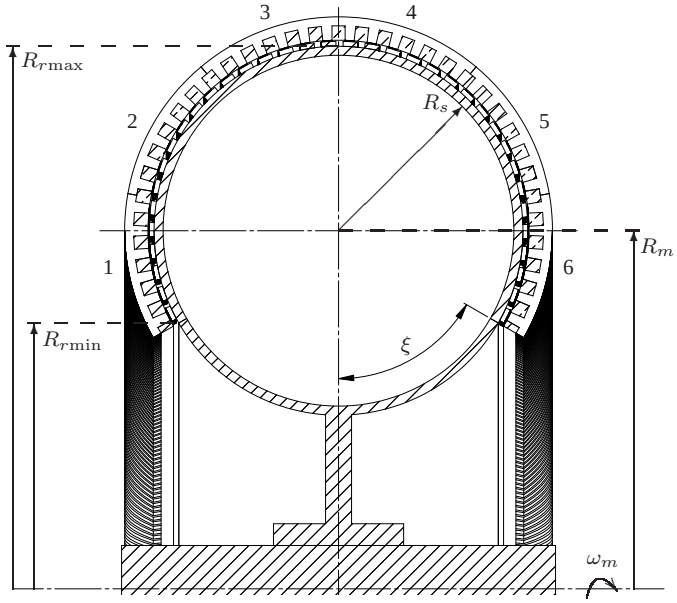

Fig. 2. Cross-section of the novel TFPM generator in the stack plane with the main dimensions, where w_m is the direction of rotation.

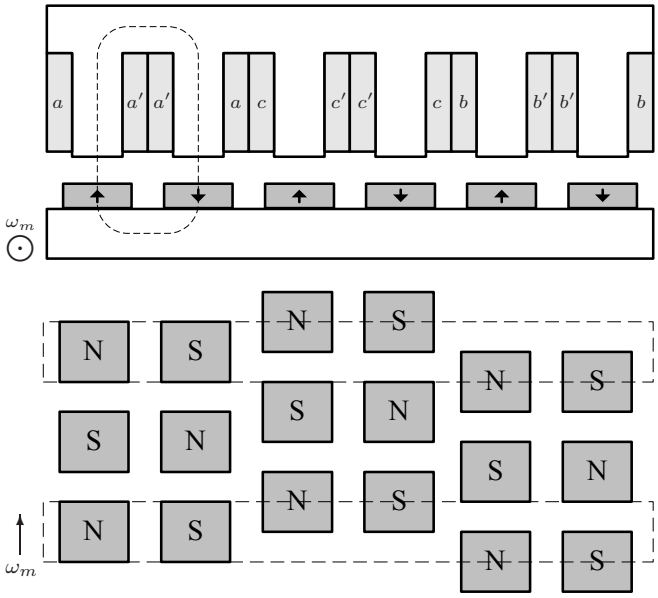

Fig. 3. Arrangement of winding in case of separated flux paths.

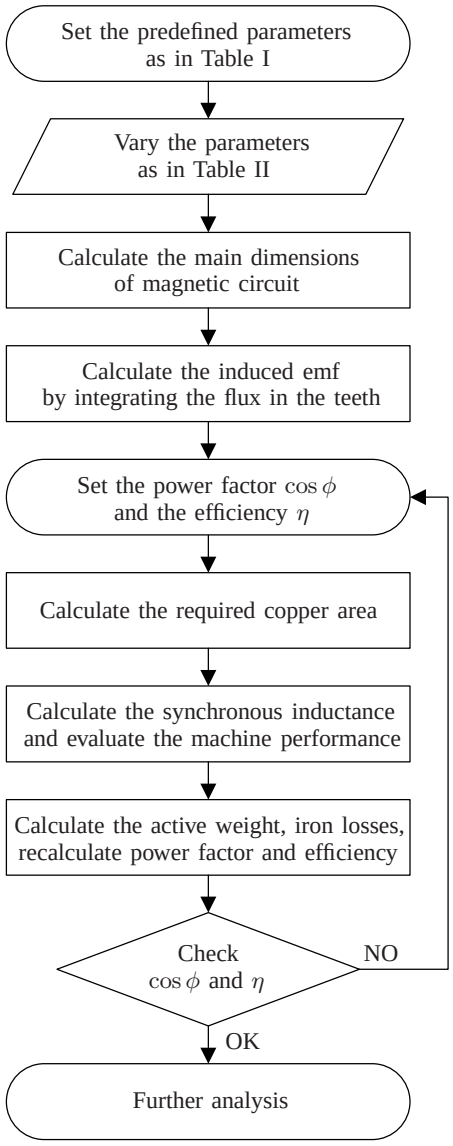

Fig. 4. Flowchart showing the design procedure of the TFPM generator.

relatively easier to analyze. The main magnet flux path is shown with a dashed line. As the winding has a three-time single phase structure it is referred to as a separated winding. The stator slots have a rectangular shape, as well as the conductors in the windings.

A more detailed description of the novel TFPM topology, as well as the design procedure applied for the parametric study of 5 MW wind turbines can be found in [7].

II. Analysis of the Novel TFPM

The calculation procedure used in the analysis of the TFPM generator is presented as a flowchart in Fig. 4. At first, the predefined parameters are set into the program as in Table I. The subject to changes design parameters are varied in ranges as shown in Table II. After that, the dimensions of the magnetic circuit and the induced emf can be calculated. To obtain the required copper area, the power factor $\cos\phi = 0.92$ and the efficiency $\eta = 0.97$ are being assumed. Once the equivalent parameters and the performance are evaluated, the active weight and the iron losses can be obtained. The new values for the power factor and the machine overall efficiency can finally be obtained. However, if the differences between the initially guessed and recalculated $\cos\phi$ and η are large (i.e. more then 5%), the corrected values should be used and the calculations be repeated.

The procedure with the equations used for analysis has been described in more details in [7]. The evaluation of the equivalent parameters has however not been presented previously and therefore is described below.

TABLE I
PREDEFINED PARAMETERS FOR 5 MW WIND TURBINE

Property	Value
Output power P_{out} (MW)	5
Number of teeth per stator stack Q_s	36
Copper losses P_{cu} (W)	$0.02P_{out}$
Turbine speed n_m (rpm)	13.2
Fill factor k_{fill}	0.55
Number of conductors in series per coil per slot n_s	1
Maximum flux density in the teeth $\widehat{B}_{ts}$ (T)	1.4
Airgap flux density B_g (T)	0.9
Magnet remanent flux density $B_{r,pm}$ (T) at 100 °C	1.1
Magnet relative permeability μ_{pm}	1.05

TABLE II
DESIGN PARAMETERS FOR 5 MW WIND TURBINE

Variable	Value
Main machine radius R_m (m)	1.5..2
Radii ratio $k_R = R_s/R_m$	0..1
Cut angle ξ (rad)	$0..\pi$
Number of poles p	400..700

A. Equivalent Parameters of the TFPM Generator

1) Main Inductance: The inductance of a coil is defined as the ratio of the flux linkage λ of this coil to the current i drawing it

$$L = \frac{\lambda}{i} = \frac{n_s \Phi}{i} = \frac{n_s^2}{\mathscr{R}}, \tag{1}$$

where Φ is the flux in the magnetic circuit with the sum reluctance $\mathscr{R}$ and n_s is the number of conductors in series per coil. The magnetic field caused by the armature reaction and the magnetic circuit are depicted in Fig. 5. By analyzing the magnetomotive force in the airgap and taking into account the mutual effect of two other phases, the main inductance L_a per each phase can be calculated as follows

$$L_a = \frac{4n_s^2}{2(\mathscr{R}_g + \mathscr{R}_{pm})} \frac{Q_s}{6} \frac{p}{2}, \tag{2}$$

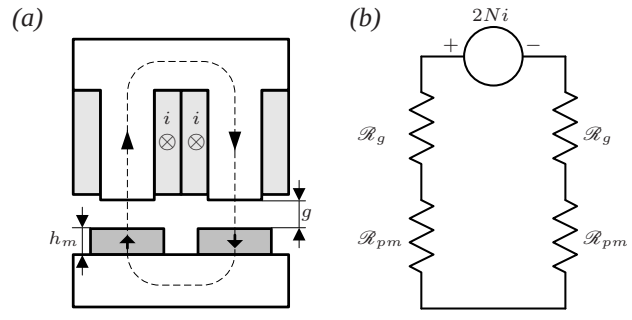

Fig. 5. Main inductance geometry *(a)* and the equivalent magnetic circuit *(b)*.

where the airgap reluctance $\mathscr{R}_g$ and the permanent magnet reluctance $\mathscr{R}_{pm}$ are given by

$$\mathscr{R}_g = \frac{g}{\mu_0 A_g} = \frac{g}{\mu_0 b_{ts1}\, l_{st,r}}, \tag{3}$$

$$\mathscr{R}_{pm} = \frac{h_m}{\mu_0 \mu_{pm} A_{pm}} = \frac{h_m}{\mu_0 \mu_{pm} l_{m,s}\, l_{m,r}}. \tag{4}$$

2) Airgap Leakage Inductance: The analysis for the airgap leakage inductance is similar to the previous case. The currents in the coils produce the magnetic field in the airgap, without entering the rotor iron, as illustrated in Fig. 6. Considering the new magnetic circuit, the airgap leakage inductance L_{ag} per phase can be found

$$L_{ag} = \frac{4n_s^2}{2\mathscr{R}'_g + \mathscr{R}_{gpm}} \frac{Q_s}{6} \frac{p}{2}, \tag{5}$$

where the reluctances $\mathscr{R}'_g$ and $\mathscr{R}_{gpm}$ can be calculated as

$$\mathscr{R}'_g = \frac{g + h_m}{2\mu_0 A_g} = \frac{g + h_m}{2\mu_0 b_{ts1}\, l_{st,r}}, \tag{6}$$

$$\mathscr{R}_{gpm} = \frac{\tau_{p,s}}{\mu_0 A_{gpm}} = \frac{\tau_{p,s}}{\mu_0 h_m\, l_{m,r}}. \tag{7}$$

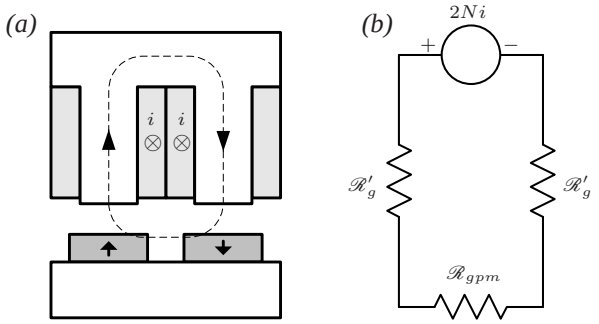

Fig. 6. Airgap leakage inductance geometry *(a)* and the equivalent magnetic circuit *(b)*.

3) Slot Leakage Inductance: The current flowing in the winding creates a magnetic field not only in the airgap, but also in the slot, as depicted in Fig. 7. This magnetic field results in the so-called slot leakage inductance. By applying the coenergy equation and integrating the magnetic field intensity in the slot volume occupied by the winding [8], the slot leakage inductance can be calculated as follows

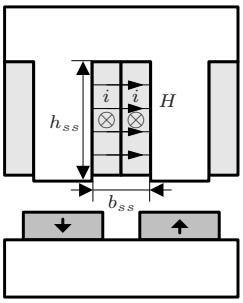

Fig. 7. Slot leakage geometry.

$$L_s = \frac{n_s^2 \mu_0 h_{ss} l_{st,r}}{3 b_{ss}} \frac{Q_s}{3} \frac{p}{2}. \tag{8}$$

4) Between-stack Inductance: The between-stack inductance is created by the magnetic field H that surrounds a conductor in the space between two neighboring stacks. If the infinitely long conductor carrying a surface current i as shown in Fig. 8*a* is assumed for simplicity, then the inductance for a conductor of length l_e and the conductor radius $R_c < r$ is given by [8]

$$L = \frac{\mu_0 l_e n_s^2}{2\pi} \ln\left(\frac{r}{R_c}\right). \tag{9}$$

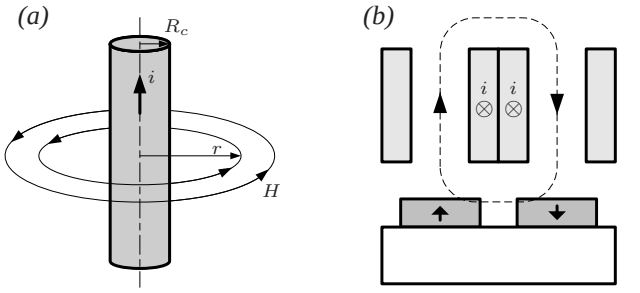

Fig. 8. Magnetic field about a cylindrical conductor *(a)* and a coil while it is between two neighboring stacks *(b)*.

For the conductor geometry and the magnetic field distribution shown in Fig. 8*b*, the effective radii and the length can be calculated as follows

$$R_c = R_{bs} = \sqrt{\frac{\tau_{p,s}(h_{ss}+b_{ts1})}{\pi}},$$
$$r = r_{bs} = \sqrt{\frac{h_{ss} b_{ss}}{\pi}},$$
$$l_e = l_{bs} = 2\,\tau_{p,r} - l_{st,r}.$$

Finally, the between-stack inductance per phase is

$$L_{bs} = \frac{\mu_0 l_{bs}\, n_s^2}{2\pi} \ln\left(\frac{r_{bs}}{R_{bs}}\right) \frac{Q_s}{3} \frac{p}{2}. \tag{10}$$

5) End-winding Inductance: The end-winding inductance is created by the magnetic field about a coil when it makes a turn between two slots, as shown in Fig. 9. The same as previously Eq. 9 is applied for derivation of the end-winding inductance. Recognize that

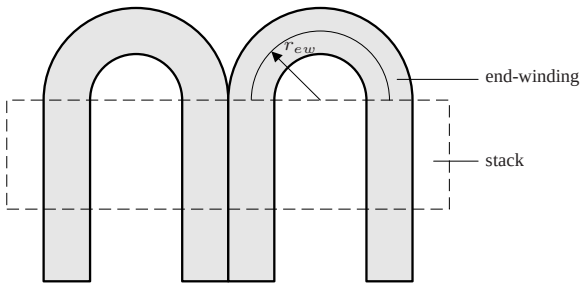

Fig. 9. End-winding geometry.

$$R_c = R_{ew} = \sqrt{\frac{b_{ss} h_{ss}}{2\pi}},$$
$$r = r_{ew} = \frac{\tau_{p,s}}{2},$$
$$l_e = l_{ew} = \frac{\pi \tau_{p,s}}{2}.$$

The end-winding inductance per each phase is calculated as

$$L_{ew} = \frac{\mu_0 \tau_{p,s} n_s^2}{4} \ln\left(\frac{\tau_{p,s}\sqrt{\pi}}{\sqrt{2 b_{ss} h_{ss}}}\right) \frac{2 Q_s}{3}, \tag{11}$$

Finally, the magnetization reactance X_{sm} and leakage reactance $X_{s\sigma}$ can be calculated

$$X_{sm} = 2\pi f_e L_a, \tag{12}$$

$$X_{s\sigma} = 2\pi f_e (L_{ag} + L_s + L_{bs} + L_{ew}), \tag{13}$$

where $f_e = n_m p/120$ is the electrical frequency with $n_m = \omega_m\, 30/\pi$ the speed of turbine in rpm.

B. Performance of the TFPM Generator

The equivalent circuit and the applied phasor diagram are presented in Fig. 10. The winding current is placed between the induced emf and the terminal voltage, so the angles are equal $\delta = \phi$. This positioning of the current would likely reduce saturation and find a reasonable compromise between the generator rating and converter rating.

When the copper area is known, the inductance of the winding can be evaluated and the new value of the power factor $\cos\phi$ can finally be obtained, as

$$\cos\phi = \frac{\sqrt{E_{ph}^2 - \left[(X_{sm} + X_{s\sigma}) I_{ph}/2\right]^2}}{E_{ph}}. \tag{14}$$

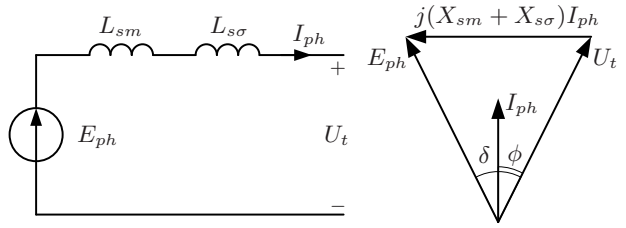

Fig. 10. The equivalent circuit and applied phaser diagram.

III. Simulation Results

A. Analyzed Characteristics

A number of characteristics have been selected in order to compare machines with different geometries and various output power. The induced emf is obtained by integrating the flux in the stator teeth produced by the magnets. This parameter is a machine size related and therefore for analysis, the induced voltage per total active weight E_{ph}/G_{total} is chosen. This characteristic would show how well the active weight of the generator is utilized. The other analyzed characteristic is the generator overall efficiency η.

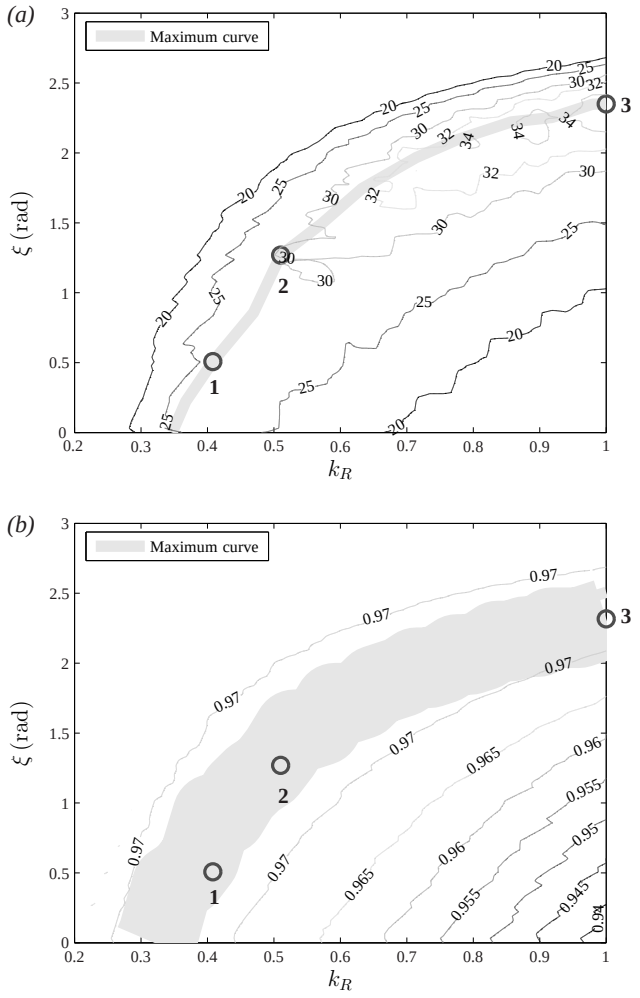

Fig. 11. Distributions of the ratio E_{ph}/G_{total} in $(10^{-3}\mathrm{V/kg})$ *(a)* and η *(b)* with respect to k_R and ξ. The maximum curves for both characteristics and three possible machine geometries denoted by circles are presented as well. The figure is plotted for machine with the following parameters: $P_{out} = 5\,\mathrm{MW}$, $R_m = 1.65\,\mathrm{m}$, $p = 660$, $Q_s = 36$.

The distribution of the ratio E_{ph}/G_{total} with respect to k_R and ξ is presented in Fig. 11*a*. Once the radii ratio k_R and the cut angle ξ reach certain level, the characteristic attains its maximum value and drops if the active weight continues to increase (i.e. when k_R increases and ξ decreases). In this case, the machine becomes somewhat oversized and, as a result, the TFPM machine looses one of its main advantageous features, i.e. high torque density. A gray stripe in Fig. 11*a* represents the maximum line, along which the machines have nearly the same total weight.

Fig. 11*b* shows the variation of η. As can be observed, the maximum line is similar to the one in Fig. 11*a*. The amount of copper in the machine is nearly constant for specified output power, as the copper losses are assumed to be constant (2% of the output power). As a result, after a certain point, the machine active weight is increasing mainly due to the increasing iron weight. The increased iron weight results in additional losses and reduced overall efficiency η of the machine.

Three machines denoted by circles in Fig. 11 were selected for more detailed analysis. The most important characteristics of these machines are summarized in Table III. The machines have different geometries, as k_R and ξ are varying, yet the machine overall efficiency η is almost the same. As can be observed, machine 2 has somewhat less total active weight and the weight of permanent magnets in machine 3 is almost twice as much as in machine 2. As the permanent magnet is one of the most expensive active materials, it makes it more advantageous to keep k_R and ξ reasonably low.

TABLE III
DATA FOR ANALYSIS

Property	1	2	3
Radii coefficient k_R	0.4082	0.5102	1.0000
Tube radius $R_m\,(\mathrm{m})$	0.6735	0.8418	1.6500
Cut angle $\xi\,(\mathrm{rad})$	0.5077	1.2693	2.3483
Total active weight $G_{total}\,(\mathrm{kg})$	36 360	34 400	36 440
Magnet weight $G_{pm}\,(\mathrm{kg})$	2 680	3 590	7 840
Efficiency η	0.97	0.97	0.97
Power factor $\cos\phi$	0.99	0.99	0.99
Induced emf $E_{ph}\,(\mathrm{V})$	975	1053	1275

Theoretically, any of machines along this maximum line could possibly be selected for further analysis. However, there is a number of constraints that should be taken into account. For example, at low values k_R and high values ξ, the machine would quite likely suffer from the increased leakage fluxes. On the other hand, the value k_R should not be too high and ξ not too low, in order to allow the mechanical attachment of the generator to the turbine shaft. There might be several machines that have the same active weight for different R_m. However, the large machine radius requires a larger nacelle and a more massive construction. Therefore, the ranges of $k_R = 0.4 - 0.8$ and $\xi = \frac{\pi}{4} - \frac{\pi}{2}$ can reasonably be selected.

B. Various Output Power

This study is conducted in order to investigate how the output power of the TFPM generator is related to the main machine radius. The chosen values for the output power, number of teeth per stator stack, and the nominal mechanical speed are summarized in Table IV.

To be able to analyze the generators with various output power, the magnetic circuit dimensions in the rotational direction should be nearly the same for all studied machines. It would help to keep the flux leakage at approximately the same level. This could be done by varying the main machine radius and the number of poles in such a way that the pole pitch in the rotational direction $\tau_{p,r}$ is nearly constant, i.e.

$$\tau_{p,r\,\max} = \frac{2\pi R_m(1+k_R)}{p} = \text{constant}. \qquad (15)$$

The main machine radius is assumed to vary in the range $R_m = (1..3)\,\mathrm{m}$, while the radii ratio k_R and the cut angle ξ remain constant, and the ratio $R_m/p = 0.0025$. The results of the simulations are demonstrated in Fig. 12.

As can be observed, the characteristic slope increases until it reaches its maximum, at which the generators have the

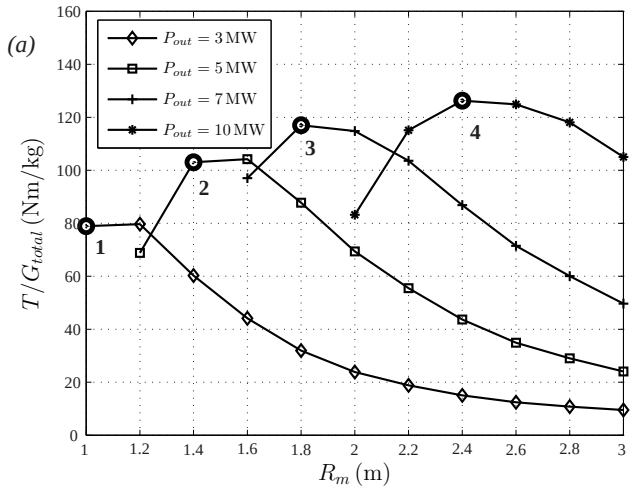

Fig. 12. Torque density (Nm/kg) with respect to the main radius R_m for turbines with the output power $P_{out} = 3, 5, 7, 10\,\mathrm{MW}$. The figure is plotted for machine with the following parameters: $\xi = \pi/3\,\mathrm{rad}$, $R_s = 0.5152\,\mathrm{m}$, $R_m/p = 0.0025$.

TABLE IV
DATA FOR ANALYSIS

Property	1	2	3	4
Fixed values:				
Output power $P_{out}\,(\mathrm{MW})$	3	5	7	10
Number of teeth Q_s	24	36	48	72
Mech. speed $n_m\,(\mathrm{rpm})$	18.6	13.2	10.6	8.3
Calculated values:				
Machine radius $R_m\,(\mathrm{m})$	1.0	1.4	1.8	2.4
Number of poles p	400	560	720	960
Active weight $G_{total}\,(\mathrm{kg})$	20 040	36 065	55 380	93 735
Magnet weight $G_{pm}\,(\mathrm{kg})$	820	2 220	4 490	11 120
Efficiency η	0.97	0.97	0.97	0.97
Power factor $\cos\phi$	0.98	0.99	0.99	0.99
Induced emf $E_{ph}\,(\mathrm{V})$	340	690	1 150	2 120
Torque density $(\mathrm{Nm/kg})$	79	103	117	126

highest torque density. It is therefore worth investigating the geometry and performance at these points in more details. The simulation results of the four machines with the different rating marked with circles in Fig. 12 are summarized in Table IV.

The obtained values for the torque density are comparable with those previously reported, for example in [9]. However, a more detailed comparison will be performed once the thermal constraints are included in the calculation procedure.

The total active weight, as well as the permanent magnet portion of the total active weight are larger for the machines with higher rating, as a result of a nonlinear dependence of the volume with the main machine radius R_m. This would likely increase the price per total weight, yet would favor a more compact design as the output power increases considerably with the main machine radius (P_{out} is approximately proportional to the cube of R_m).

It should also be mentioned that the mechanical constraints would limit the maximum allowed size of the generator, as the increased generator weight would increase the inactive portion of the nacelle weight and as a result require a more massive tower construction.

IV. CONCLUSIONS

The analytical method for the evaluation of the synchronous inductance in the TFPM has been developed and applied for the evaluation of machine performance. Different machine geometries have been analyzed. It has been found that there is a number of machines with various ξ and k_R that have approximately the same performances. Therefore, some new constraints have been added and the optimal ranges for further analysis have been suggested.

Furthermore, the machine performance has also been evaluated for the output power $3, 5, 7, 10\,\mathrm{MW}$. It was found that the torque density turns to improve with the increasing output power of the generator.

In order to improve the analytical calculations of inductances, the three-dimensional finite element analysis is required. This study will also help to analyze more thoroughly the influence of the dimensions of magnetic circuite on the flux leakage.

For the performed analysis, it was assumed that all the heat produced by losses can be extracted from the machine. This might however not be a case in reality and the thermal model should therefore be included in the calculations.

In order to investigate in more details the influence of the machine radius R_m and the cut angle ξ on the mechanical strength of the generator and the total weight of the system, the analysis of the mechanical structure (i.e. shaft, bearings, fastening) should be considered as well.

Finally, to verify the developed model, a downscaled prototype is under development, the measurements to be performed and compared with analytical results.

REFERENCES

[1] *Wind power in power systems*, edited by T. Ackermann, John Wiley & Sons, 2005.
[2] H. Polinder, F.F.A. van der Pijl, G.J. de Vilder, and P. Tavner, "Comparison of direct-drive and geared generator concepts for wind turbines", in *Proc IEEE Int. Conf. Electric Machines and Drives*, San Antonio, USA, 2005, pp. 543-550.
[3] H. Weh, H. Hoffmann, J. Landrath, "New permanent magnet excited synchronous machine with high efficiency at low speeds", in *Proc. Int. Conf. Electrical Machines*, Vol. 3, Pisa, Italy, 1990, pp. 35-40.
[4] H. Weh, H. May, "Achievable force densities for permanent magnet excited machines in new configurations", in *Proc. Int. Conf. Electrical Machines*, Munich, Germany, 1986, pp. 1107-1111.
[5] G. Henneberger and M. Bork, "Development of a new transverse flux motor", *IEE Colloquium on New Topologies for Permanent Magnet Machines*, Digest No. 1997/090, 1997, pp. 1/1-1/6.
[6] H. Polinder, S.W.H. de Haan, M.R. Dubois, and J.G. Slootweg, "Basic operation principles and electrical conversion systems of wind turbines", in *Proc. Nordic Workshop on Power and Industrial Electronics*, Trondheim, Norway, 2004.
[7] D. Svechkarenko, J. Soulard, and C. Sadarangani, "A novel transverse flux generator in direct-driven wind turbines", in *Proc. Nordic Workshop on Power and Industrial Electronics*, Lund, Sweden, 2006.
[8] D. Hanselman, *Brushless permanent magnet motor design*, Second edition, The Writers Collective, 2003.
[9] A. Grauers, "Design of direct-driven permanent-magnet generators for wind turbines", PhD thesis, Chalmers University of Technology, Sweden, 1996.